# Strain and temperature measurement discrimination with forward Brillouin scattering in optical fibers

## L. A. SÁNCHEZ,[1] ⓘ A. DÍEZ,[1,2,*] ⓘ J. L. CRUZ,[1,2] AND M. V. ANDRÉS[1,2] ⓘ

[1]*Laboratory of Fiber Optics, ICMUV, Universidad de Valencia, Dr. Moliner 50, 46100, Spain*
[2]*Departamento de Física Aplicada y Electromagnetismo, Universidad de Valencia, Dr. Moliner 50, 46100, Spain*
[*]*antonio.diez@uv.es*

**Abstract:** A novel method that enables simultaneous and discriminative measurement of strain and temperature using one single optical fiber is presented. The method is based on the properties of transverse acoustic mode resonances (TAMRs) of the optical fiber. In particular, it is based on the different sensitivity to temperature and strain that exhibit the radial modes $R_{0,m}$ and a family of torsional-radial modes denoted as $TR_{2,m}^{(1)}$. We show that the resonance frequencies of both types of resonances shift linearly with temperature and strain, but at different rates. By the combined use of the different sensitivities of the two families of TAMRs, we experimentally demonstrate discriminative measurements of strain and temperature. A detection limit of strain and temperature better than 25 µε and 0.2 °C is achieved.

## 1. Introduction

Optical fiber sensing (OFS) technologies have experienced a fast growth in the last decades, with applications in many fields. In particular, fiber optics are a suitable platform for sensing a number of physical properties. The feasibility of strain and temperature measurements enable their application, for example, in the monitoring of infrastructures [1]. However, many fiber optic based optical sensors cannot inherently discriminate between strain and temperature since both magnitudes often affect similarly to the physical principle in which the sensor relies. To overcome this limitation, different strategies adapted to each specific type of sensor have been developed. For instance, in fiber grating-based optical sensors, many temperature and strain discriminating techniques have been proposed. Most schemes involve two independent measurements with two gratings [2–6], although methods for discrimination between temperature and strain using a single fiber grating have also been reported [7–9].

Discrimination between temperature and strain is also an issue in Brillouin fiber-optic distributed sensors, since the Brillouin frequency shift depends linearly on both, strain and temperature. Different solutions have been proposed to develop this type of sensors with discrimination capacity using a single fiber. Most rely on the use of specialty optical fibers such as PM fibers [10], $Er^{3+}$-doped fibers [11], or few-mode optical fibers [12]. However, it should be noted that often the measurement procedures required by these methods are technically complex.

In this work, we show that measurement and fully discrimination between strain and temperature using a conventional optical fiber can be accomplished based on the effect of forward stimulated Brillouin scattering (FSBS). FSBS is an optomechanic effect that occurs when light is scattered by transverse acoustic mode resonances (TAMRs) of the optical fiber, which are excited through electrostriction by an optical pump wave. Recently, innovative sensing developments and applications based on FSBS have boosted the interest of FSBS as physical mechanism for fiber sensing. FSBS depends on the fiber properties but also on the fiber surroundings, which widens

the sensing capabilities [13,14]. Additionally, distributed fiber sensing based on FSBS has been demonstrated [15–17].

The characteristic frequencies of TAMRs of an optical fiber are dependent on the fiber properties, in particular, on temperature [18] and strain [19,20]. The TAMRs behind FSBS in standard optical fibers are radial modes $R_{0,m}$ and torsional-radial modes $TR_{2,m}$ [21], which can be excited by the electrostriction generated with optical pump pulses. Most of the applications based on TAMRs reported so far rely on the properties of either $R_{0,m}$ or $TR_{2,m}$ acoustic resonances. In this work, we show that discriminative measurement of strain and temperature can be accomplished by taking into account and combining the response of both type of resonances. The key point of this work relies on the different response that $R_{0,m}$ modes and a subgroup of $TR_{2,m}$ modes exhibit to those physical magnitudes. The approach reported in this paper relies on radio frequency measurements in the range of hundreds of MHz, which can be done very accurately with relatively low-cost equipment. Moreover, the resonances exhibit high Q values. Therefore, a remarkable accuracy is achieved in the acquisition of the raw experimental data before the computation of temperature and strain. The sensor here presented is compatible with wavelength multiplexing techniques.

## 2. Fundamentals

The resonance frequencies of $R_{0,m}$ and $TR_{2,m}$ modes in an optical silica fiber can be computed by solving the corresponding characteristic equations [22]. These frequencies depend on the fiber radius $a$ and on the longitudinal and shear acoustic velocities in silica, $V_L$ and $V_S$, respectively. The $TR_{2,m}$ mode spectrum includes two families of torsional-radial modes with different properties, which we denoted as $TR_{2,m}^{(1)}$ and $TR_{2,m}^{(2)}$ [23]. The first series, $TR_{2,m}^{(1)}$ modes, are acoustic mode resonances whose displacement field contains a predominant azimuthal component, while in the case of $TR_{2,m}^{(2)}$ modes the main component of the displacement vector is the radial component. Approximated analytical expressions for the resonance frequencies of the acoustic modes were derived in [23]. For large mode orders ($m > 3$ for $R_{0,m}$ modes and $m > 10$ for $TR_{2,m}$ modes) the resonance frequencies $f_{R_{0,m}}, f_{TR_{2,m}^{(1)}}$, and $f_{TR_{2,m}^{(2)}}$ can be accurately approximated –with a relative error below 1‰– by the following expressions,

$$f_{R_{0,m}} \simeq \frac{V_L}{2\pi a} \left( z_m - \frac{16\,\alpha^2}{8\,z_m} \right) \tag{1}$$

$$f_{TR_{2,m}^{(1)}} \simeq \frac{V_S}{2\pi a} \left( z_m - \frac{15}{8\,z_m} \right) \tag{2}$$

$$f_{TR_{2,m}^{(2)}} \simeq \frac{V_L}{2\pi a} \left( z_m - \frac{15}{8\,z_m} \right) \tag{3}$$

where $\alpha = V_S/V_L$ and $z_m = m \cdot \pi - \pi/4$, being $m$ an integer that indicates the in $\alpha = V_S/V_L$ dex that indicates the mode order. By analyzing Eqs. (1)-(3), we can infer several key features that were confirmed experimentally. First, the linear dependence of the resonance frequencies with temperature and strain can be inferred since, for silica, the parameters $V_L$, $V_S$ and $a$ depend linearly with temperature and strain, for small changes of those magnitudes. Second, for large values of $m$, the contribution of the second term inside the parenthesis in Eqs. (1)-(3) is small and the resonance frequencies of $R_{0,m}$ and $TR_{2,m}^{(2)}$ modes tend to be equal, and they are proportional to $V_L$, while the resonance frequencies of $TR_{2,m}^{(1)}$ modes are proportional to $V_S$. The temperature sensitivity and the strain sensitivity of $V_L$ and $V_S$ are different. Therefore, the dependence of the resonance frequencies of $R_{0,m}$ and $TR_{2,m}^{(2)}$ on the one hand, and $TR_{2,m}^{(1)}$ on the other hand, on changes of temperature and strain will be different as well. The technique proposed in this

paper for the measurement and discrimination between strain and temperature is based on the differential sensitivity of $R_{0,m}$ and $TR_{2,m}^{(1)}$ mode resonances to those magnitudes.

As mentioned above, in a wide range of variation of temperature and strain, the frequency shift of $R_{0,m}$ and $TR_{2,m}^{(1)}$ modes changes linearly with those magnitudes, but they do it at different rates. Then, with respect to the frequency values of an unstrained fiber at room temperature, the relative frequency shifts of an $R_{0,m}$ mode and a $TR_{2,m}^{(1)}$ mode ($\Delta f_R/f_R$, $\Delta f_{TR}/f_{TR}$) in a fiber subjected to a change of temperature $\Delta T$ and strain $\Delta\varepsilon$, can be expressed, respectively, as:

$$\left(\frac{\Delta f_R}{f_R}\right) = c_R^\varepsilon \cdot \Delta\varepsilon + c_R^T \cdot \Delta T \tag{4}$$

$$\left(\frac{\Delta f_{TR}}{f_{TR}}\right) = c_{TR}^\varepsilon \cdot \Delta\varepsilon + c_{TR}^T \cdot \Delta T \tag{5}$$

where $c_R^\varepsilon$ and $c_R^T$ are the temperature and strain coefficients of radial modes, and $c_{TR}^\varepsilon$ and $c_{TR}^T$. are the temperature an strain coefficients of torsional-radial modes of the $TR_{2,m}^{(1)}$ family. It is worthwhile to underline here that, according to Eqs. (1)-(2), all resonances of a given series exhibit the same slope, as stated in Eqs. (4) and (5). Then, by solving (4) and (5), changes of temperature and strain can be simultaneously obtained from the measurement of frequency shifts of $R_{0,m}$ and $TR_{2,m}^{(1)}$ modes.

The errors for the discriminated temperature $e_{\Delta T}$ and strain $e_{\Delta\varepsilon}$ can be obtained as follows [24],

$$e_{\Delta T} = \frac{\sqrt{(c_{TR}^\varepsilon \cdot e_R)^2 + (c_R^\varepsilon \cdot e_{TR})^2}}{|c_{TR}^T \cdot c_R^\varepsilon - c_{TR}^\varepsilon \cdot c_R^T|} \tag{6}$$

$$e_{\Delta\varepsilon} = \frac{\sqrt{(c_{TR}^T \cdot e_R)^2 + (c_R^T \cdot e_{TR})^2}}{|c_{TR}^T \cdot c_R^\varepsilon - c_{TR}^\varepsilon \cdot c_R^T|} \tag{7}$$

where $e_R$ and $e_{TR}$ represent the standard deviation of the relative frequency shift measurements of radial and torsional-radial modes, respectively. In the derivation of Eqs. (6) and (7), the uncertainty in the temperature and strain coefficients have been neglected; only the uncertainty of the frequency shift measurement of the TAMRs has been taken into account.

## 3. Experimental procedures

### 3.1. *Experimental arrangement*

We investigated experimentally the resonance frequencies of TAMRs in a single-mode optical fiber, as well as their dependence on temperature and strain using a long-period grating (LPG) assisted pump-and-probe method [25]. Figure 1 shows a diagram of the experimental arrangement. The fiber used in the experiments was the SM1500 (4.2/125) from Fibercore. TAMRs were excited in the optical fiber through electrostriction by optical pump pulses provided by a Q-switched microchip laser (TEEM Photonics SNP-20F-100, 700 ps pulse duration, 1064 nm wavelength, 19.9 kHz repetition rate). The pump laser was delivered into the fiber using a ×16 aspheric lens and a 3-axis positioning stage. A half-wave plate (HWP) was used to adjust the polarization of the pump beam in order to control the excitation of torsional-radial modes.

The TAMRs generated in the fiber were detected by means of a narrow-band (LPG) that was written in the core of the fiber. The polymer coating was stripped before LPG inscription. Removing of the polymer coating facilitates the LPGs inscription process. Moreover, it leads to narrower acoustic resonances since conventional polymer coatings cause acoustic damping.

The period of the LPG was 52.3 µm, the length was 11 cm. The LPG exhibits a transmission notch of –9 dB, centered at 1551 nm, and its bandwidth was 1.3 nm. A detailed description of
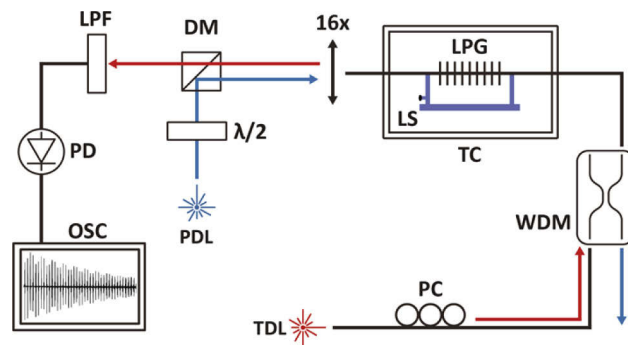
**Fig. 1.** Experimental setup. PD: photodetector; LPF: long-pass filter; DM: dichroic mirror; WDM: wavelength division multiplexer; TC: temperature chamber; LS: linear stage; PC: polarization controller; WDM: wavelength division multiplexer; PDL: pump laser; TDL: probe laser.

the LPG fabrication method can be found in [26]. The excited TAMRs modulate slightly the LPG's properties through the photo-elastic effect, which causes an oscillatory shift of the LPGs resonance wavelength. The LPG was interrogated using a probe laser (Keysight 81940 A) tuned to one edge of the LPG notch. The probe signal was detected by a fast photodetector (Newport 1611FC-AC) and recorded by an oscilloscope (Keysight DSOS104A). The frequencies of the different TAMRs were obtained by calculating the Fourier transform of the probe temporal trace.

Measurements as a function of temperature were performed by placing the section of fiber with the LPG in a cooling-heating temperature chamber (WTB Binder MK 53). The temperature range covered in the experiments was from $-20°$ to 80 °C, with a temperature accuracy of 0.1 °C. Measurements as a function of strain were performed by stretching the LPG using a linear stage. The strain response was measured in the range of 0-1.5 mε, with a strain resolution of 10 με. Notice that the LPG exhibits its own sensitivity to changes of temperature and strain. Therefore, to carry out the characterization of the TAMRs with temperature/strain, the probe laser wavelength was tuned accordingly to follow the LPG shift.

### 3.2. Experimental results

Figure 2(a) shows an example of the temporal trace of the probe signal after one pump pulse passed through the fiber with the LPG. The first 20 ns of the temporal trace were discarded since it includes the contribution of the instantaneous fiber response due to Kerr nonlinearity [25]. The temporal trace contains a series of oscillations with amplitude decaying with time. The polarization orientation of the pump was adjusted to favor the simultaneous excitation of both $R_{0,m}$ and $TR_{2,m}$ modes. Two series of oscillations can be distinguished, a periodic pattern of oscillations separated by ~21 ns that results from the interaction of $R_{0,m}$ modes with the LPG, and a second periodic pattern of oscillations separated ~33 ns that is caused by $TR_{2,m}$ modes.

The RF spectrum of the probe signal contains a series of peaks located at the resonance frequencies of the different acoustic mode resonances that are excited by the pump. Figure 2(b) shows the spectrum between 200 MHz and 600 MHz at 20 °C and no strain. The different peaks are labelled according to the mode series to which they belong.

To obtain the temperature and strain coefficients of modes $R_{0,m}$ and $TR_{2,m}^{(1)}$, we performed two different experiments. First, we carried out measurements at different temperatures and no strain. In a second row, measurements were performed at room temperature and the strain applied to the fiber was varied. We limit the analysis to $R_{0,m}$ modes with $m > 3$ and $TR_{2,m}^{(1)}$ modes with $m > 10$. Figure 3 shows the spectrum of the $R_{0,10}$ and the $TR_{2,15}^{(1)}$ acoustic modes for different
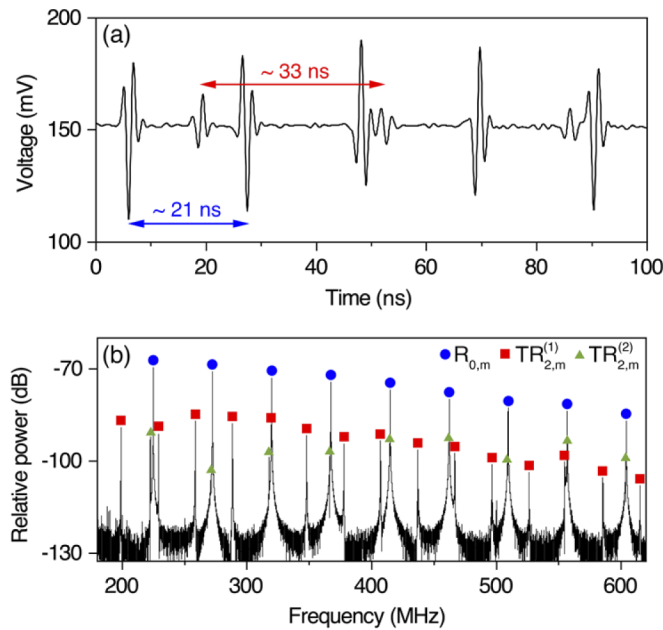
**Fig. 2.** (a) Temporal trace of the probe signal when a pump pulse propagates through the LPG. (b) RF spectrum of the probe signal from 200 MHz to 600 MHz. Each peak corresponds to a TAMR. Symbols indicate the series to which each TAMR belongs. Average pump power: 30 mW (peak power: 2.25 kW)

temperatures and no strain (Fig. 3 (a)-(c)), and for different values of strain at room temperature (Fig. 3 (b)-(d)). In both cases, the increase of temperature or strain shifts the peaks to higher frequencies. The resonance frequencies of the different TAMRs were obtained from the RF spectra by curve-fitting a Lorentzian function to each peak. It is worthwhile to outline here that the resonances exhibit typical $Q$ values higher than $2 \times 10^3$, enabling an accurate determination of the resonant frequencies.

Figures 4(a) and 4(b) shows the relative frequency shift $\Delta f/f$ for the $R_{0,10}$ and $TR_{2,15}^{(1)}$ resonances as a function of temperature and strain, respectively. The relative frequency shift $\Delta f/f$ of all modes belonging to a given series –either $R_{0,m}$ or $TR_{2,m}^{(1)}$ modes– was the same within the experimental error, as one can derive from Eqs. (1)–(3). The solid line included in Figs. 4(a) and 4(b) results from performing a linear fitting of the relative frequency shift values including all modes of the corresponding mode series. This feature provides the possibility of using the relative frequency shift average taking into account all modes of each series to obtain $\Delta T$ and $\Delta\varepsilon$, which can help to improve the accuracy.

### 3.3. Discussion

In the range of temperature and strain that was analyzed, all the dependencies of the frequency shift of the different TAMRs show excellent linearity; thus by linear fitting, we can get the strain coefficient and the temperature coefficient of the different $R_{0,m}$ modes and $TR_{2,m}^{(1)}$ modes. Table 1 summarizes the obtained results.

The temperature and strain accuracies can be estimated through Eqs. (6) and (7) by taking into account the standard deviation of the relative frequency shift measurements. Taking into account the characteristics of our measurement equipment and after repeated experiments were performed, the uncertainty in the determination of frequency shift values $\Delta f$ was estimated to be
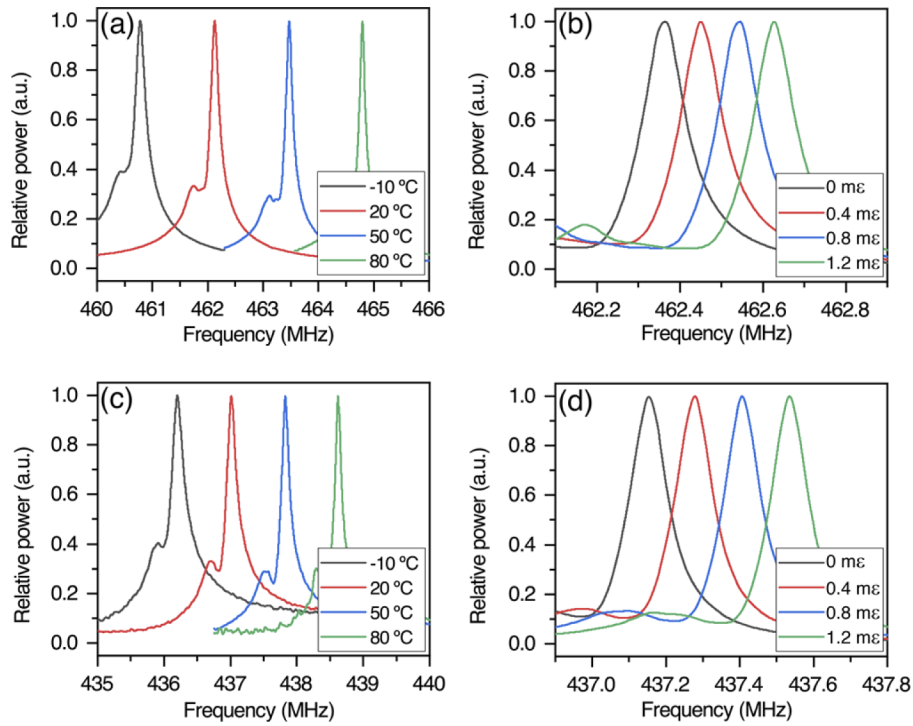
**Fig. 3.** RF spectrum of a TAMR, for different values of temperature and strain. (a) and (b) correspond to $R_{0,10}$; (c) and (d) correspond to $TR_{2,15}^{(1)}$.
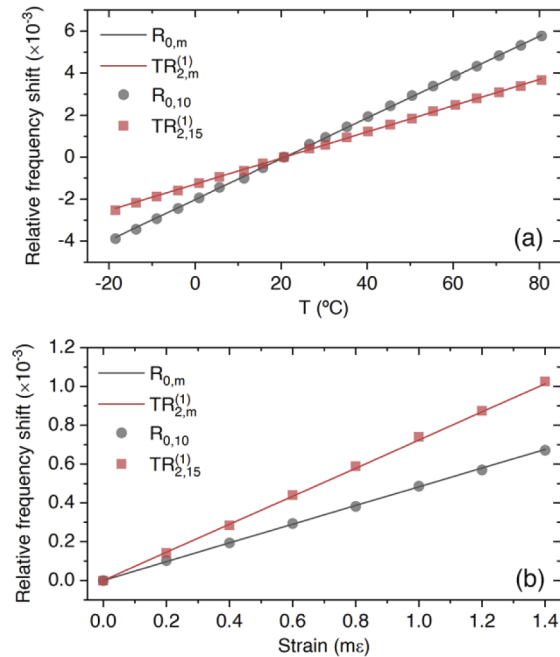


**Fig. 4.** Relative frequency shift of TAMRs as a function of (a) temperature and (b) strain. Symbols are for experimental values of $R_{0,10}$ and $TR_{2,15}^{(1)}$ modes respectively. Solid lines show the linear fit of averaged values of $\Delta f/f$ over all the resonances of each series.

**Table 1. Temperature and strain coefficients of the radial modes $R_{0,m}$ and torsional-radial modes $TR_{2,m}^{(1)}$**

| $c_R^T$ (°C$^{-1}$) | $c_R^\varepsilon$ (µε$^{-1}$) | $c_{TR}^T$ (°C$^{-1}$) | $c_{TR}^\varepsilon$ (µε$^{-1}$) |
|---|---|---|---|
| $(9.73 \pm 0.04) \times 10^{-5}$ | $(4.82 \pm 0.03) \times 10^{-7}$ | $(6.24 \pm 0.04) \times 10^{-5}$ | $(7.25 \pm 0.03) \times 10^{-7}$ |

better than 4 kHz. The standard deviation of the relative frequency shift $\Delta f / f$ measurements is different for the different TAMRs since it depends on frequency; in particular, it decreases with frequency. As a result, the temperature and strain accuracy vary slightly depending on the specific TAMR used to evaluate $\Delta T$ and $\Delta \varepsilon$. As an example, the standard deviation of $\Delta f / f$ for the $R_{0,10}$ and $TR_{2,15}^{(1)}$ is ~$9 \times 10^{-6}$, which could be used to estimate the temperature and strain accuracies by using Eqs. (6) and (7) as $\pm 0.2$ °C in temperature and $\pm 25$ µε in strain. Note that temperature and strain accuracies improves when higher order TAMRs are used to estimate $\Delta T$ and $\Delta \varepsilon$.

We performed an experiment to validate our approach. We measured the frequencies of two pair of resonances ($R_{0,10}$, $R_{0,20}$, $TR_{2,15}^{(1)}$, and $TR_{2,24}^{(1)}$) at room temperature ($20.6 \pm 0.1$ °C) and no strain. Then, we applied to the fiber a temperature of $62.0 \pm 0.1$ °C and a strain of $900 \pm 10$ µε and we measured the frequency shift of these resonances. Table 2 summarizes the results. The values of temperature and strain obtained when solving Eqs. (4)–(5) with frequencies of $R_{0,10}$ and $TR_{2,15}^{(1)}$ modes are 887 µε and 61.9 °C. Using frequencies of modes $R_{0,20}$ and $TR_{2,24}^{(1)}$ the values of strain and temperature are 62.2 °C and 909 µε. Both values being within the errors limits established by our analysis.

**Table 2. Frequencies of different modes at two conditions of strain and temperature**

| | f (MHz) | |
|---|---|---|
| | *20.6 °C, 0 µε* | *62.0 °C, 900 µε* |
| $R_{0,10}$ | 462.126 | 464.180 |
| $R_{0,20}$ | 935.032 | 939.226 |
| $TR_{2,15}^{(1)}$ | 437.014 | 438.421 |
| $TR_{2,24}^{(1)}$ | 704.837 | 707.131 |

As mentioned above, the fiber used in the experiments was the SM1500 (4.2/125) from Fibercore. We chose such fiber because it made simple for us the fabrication of the narrowband LPG. However, any other type of single-mode silica optical fiber with the same diameter will provide similar results. Notice that the acoustic properties of optical fibers are essentially determined by the fiber cladding.

The properties of the sensor rely essentially on the acoustic properties of the optical fiber, and on how they depend on temperature and strain. The LPG is used just to interrogate the TAMRs, so other interrogation methods are also possible. For example, a fiber Bragg grating (FBG) can be used instead of a LPG. Both alternatives, LPG and FBG, enable a straightforward implementation of wavelength multiplexing allowing the development of a multipoint sensing.

Table 3 summarizes the results reported in this paper along with the performance of different methods presented in the literature. In general terms, we can state that the sensitivity and accuracy of the results reported here are of the same order of magnitude than what it has been demonstrated by other methods that provide temperature and strain discrimination using optical fibers. However, we believe that accuracy can still be enhanced by improving the experimental arrangement, and the procedure to obtain the frequencies' shift. In addition, the present proposal, being a frequency encoded sensor system, can be advantageous in comparison with common fiber

sensors based on the measurement of wavelength and in comparison with Brillouin scattering measurements. The equipment required by our approach is a simple oscilloscope with a built-in fast Fourier transform, while other techniques require an optical spectrum analyzer and/or more specific electronic equipment.

**Table 3. Comparative of different methods for discriminative measurement of strain and temperature using optical fibers**

| Ref. / Measuring technique | Strain / Temperature range | Strain / Temperature accuracy | Fiber length |
|---|---|---|---|
| Present work / FSBS | 0–1400 με / -20–80 °C | ± 25 με / ± 0.2 °C | 11 cm |
| [2] / Two superimposed FBGs | 0–600 με / 10–60 °C | ± 10 με / ± 5 °C | |
| [3] / FBG + LPG | 290–1270 με / 25–50 °C | ± 9 με / ± 1.5 °C | >3.5 cm |
| [4] / FBG in PANDA fiber | 0–1100 με / 0–100 °C | ± 20 με / ± 2 °C | |
| [5] / FBGs in undoped and boron doped fibers | 0–1000 με / 30–130 °C | ± 18.4 με / ± 2.2 °C | < 15 mm |
| [6] / Laser-notched LPGs | 0–1820 με / 20–200 °C | ± 21 με / ± 0.3 °C | 11.5 cm |
| [8] / Multiple bands in LPG | 0–2100 με / 0–125 °C | ± 58 με / ± 1 °C | |
| [9] / FBG in Hi-Bi fiber | 0–4000 με / 30–70 °C | ± 60 με / ± 6 °C | 1 cm |
| [10] / Brillouin Scatter. in PANDA fiber | 0–1500 με / 10–70 °C | ± 3 με / ± 0.08 °C | 31 m |
| [11] / Brillouin Scatter. + fluorescence in Er-doped fiber | 0–4000 με / 30–100 °C | ± 300 με / ± 4 °C | 60 cm |

## 4. Conclusions

Discriminative measurement of strain and temperature using an approach fully based on opto-mechanical interaction in optical fibers is demonstrated. The method is based on the properties of transverse acoustic mode resonances in optical fibers, in particular, on the different sensitivity to changes of temperature and strain of radial modes $R_{0,m}$ and the series $TR_{2,m}^{(1)}$ of torsional-radial modes. TAMRs were excited optically and monitored by means of a long-period grating. The frequency shift of the two type of TAMRs was calibrated against strain and temperature. It is shown that the relative frequency shift is the same for all modes of a given series. Taking into account the accuracy provided by our experimental arrangement as well as the procedure to obtain the resonance frequency of the TAMRs, we have estimated and demonstrated that temperature and strain can be obtained with accuracies better than ± 0.2 °C in temperature and ± 25 με in strain. The accuracy obtained with our measuring approach clearly benefits from having the information encoded in the frequency domain, on the one hand, and using acoustic resonances with high Q values, on the other hand. Our proposal is fully compatible with common wavelength multiplexing techniques based on LPG and FBG.

**Disclosures.** The authors declare no conflicts of interest.

**Data availability.** Data underlying the results presented in this paper are not publicly available at this time but may be obtained from the authors upon reasonable request.

### References

1. H. E. Joe, H. Yun, S. H. Jo, M. B. G. Jun, and B. K. Min, "A Review on Optical Fiber Sensors for Environmental Monitoring," Int. J. of Precis. Eng. and Manuf.-Green Tech. **5**(1), 173–191 (2018).
2. M. G. Xu, J.-L. Archambault, L. Reekie, and J. P. Dakin, "Discrimination between strain and temperature effects using dual-wavelength fiber grating sensors," Electron. Lett. **30**(13), 1085–1087 (1994).

3.  H. J. Patrick, G. M. Williams, A. D. Kersey, J. P. Pedrazzani, and A. M. Vengsarkar, "Hybrid fiber Bragg grating/long period fiber grating sensor for strain/temperature discrimination," IEEE Photonics Technol. Lett. **8**(9), 1223–1225 (1996).
4.  M. Sudo, M. Nakai, K. Himeno, S. Suzaki, A. Wada, and R. Yamauchi, "Simultaneous Measurement of Temperature and Strain using PANDA Fiber Grating," in *12th International Conference on Optical Fiber Sensors*, Vol. 16 of 1997 OSA Technical Digest Series (Optica Publishing Group, 1997), paper OWC7.
5.  P. M. Cavaleiro, F. M. Araújo, L. A. Ferreira, J. L. Santos, and F. Farahi, "Simultaneous measurement of strain and temperature using Bragg gratings written in germanosilicate and boron-codoped germanosilicate fibers," IEEE Photonics Technol. Lett. **11**(12), 1635–1637 (1999).
6.  H. Zeng, T. Geng, W. Yang, M. An, J. Li, F. Yang, and L. Yuan, "Combining Two Types of Gratings for Simultaneous Strain and Temperature Measurement," IEEE Photonics Technol. Lett. **28**(4), 477–480 (2016).
7.  Y. Kim, Y. W. Lee, and B. Lee, "Simultaneous measurement of strain and temperature using phase-shifted long-period grating written on polarization-maintaining fiber," in *Optical Fiber Sensors, OSA Technical Digest* (CD) (Optica Publishing Group, 2006), paper TuE82.
8.  V. Bhatia, D. Campbell, R. O. Claus, and A. M. Vengsarkar, "Simultaneous strain and temperature measurement with long-period gratings," Opt. Lett. **22**(9), 648–650 (1997).
9.  S. T. Oh, W. T. Han, U. C. Paek, and Y. Chung, "Discrimination of temperature and strain with a single FBG based on the birefringence effect," Opt. Express **12**(4), 724–729 (2004).
10. W. Zou, Z. He, and K. Hotate, "Complete discrimination of strain and temperature using Brillouin frequency shift and birefringence in a polarization-maintaining fiber," Opt. Express **17**(3), 1248–1255 (2009).
11. M. Ding, Y. Mizuno, and K. Nakamura, "Discriminative strain and temperature measurement using Brillouin scattering and fluorescence in erbium-doped optical fiber," Opt. Express **22**(20), 24706–24712 (2014).
12. Y. Weng, E. Ip, Z. Pan, and T. Wang, "Single-end simultaneous temperature and strain sensing techniques based on Brillouin optical time domain reflectometry in few-mode fibers," Opt. Express **23**(7), 9024–9039 (2015).
13. Y. Antman, A. Clain, Y. London, and A. Zadok, "Optomechanical sensing of liquids outside standard fibers using forward stimulated Brillouin scattering," Optica **3**(5), 510–516 (2016).
14. D. M. Chow and L. Thévenaz, "Forward Brillouin scattering acoustic impedance sensor using thin polyimide-coated fiber," Opt. Lett. **43**(21), 5467–5470 (2018).
15. D. M. Chow, Z. Yang, M. A. Soto, and L. Thévenaz, "Distributed forward Brillouin sensor based on local light phase recovery," Nat. Commun. **9**(1), 2990 (2018).
16. G. Bashan, H. H. Diamandi, Y. London, E. Preter, and A. Zadok, "Optomechanical time-domain reflectometry," Nat. Commun. **9**(1), 2991 (2018).
17. C. Pang, Z. Hua, D. Zhou, H. Zhang, L. Chen, X. Bao, and Y. Dong, "Opto-mechanical time-domain analysis based on coherent forward stimulated Brillouin scattering probing," Optica **7**(2), 176–184 (2020).
18. Y. Tanaka and K. Ogusu, "Tensile-strain coefficient of resonance frequency of depolarized guided acoustic-wave Brillouin scattering," IEEE Photonics Technol. Lett. **11**(7), 865–867 (1999).
19. Y. Tanaka and K. Ogusu, "Temperature coefficient of sideband frequencies produced by depolarized guided acoustic-wave Brillouin scattering," IEEE Photonics Technol. Lett. **10**(12), 1769–1771 (1998).
20. N. Hayashi, K. Suzuki, S. Y. Set, and S. Yamashita, "Temperature coefficient of sideband frequency produced by polarized guided acoustic-wave Brillouin scattering in highly nonlinear fibers," Appl. Phys. Express **10**(9), 092501 (2017).
21. A. S. Biryukov, M. E. Sukharev, and E. M. Dianov, "Excitation of sound waves upon propagation of laser pulses in optical fibres," Quantum Electron. **32**(9), 765–775 (2002).
22. R. N. Thurston, "Elastic waves in rods and optical fibers," Journal of Sound and Vibration **159**(3), 441–467 (1992).
23. L. A. Sánchez, A. Díez, J. L. Cruz, and M. V. Andrés, "High accuracy measurement of Poisson's ratio of optical fibers and its temperature dependence using forward-stimulated Brillouin scattering," Opt. Express **30**(1), 42–52 (2022).
24. J. R. Taylor, *An Introduction to Error Analysis* (University Science Books, 1997).
25. L. A. Sánchez, A. Díez, J. L. Cruz, and M. V. Andrés, "Efficient interrogation method of forward Brillouin scattering in optical fibers using a narrow bandwidth long-period grating," Opt. Lett. **45**(19), 5331–5334 (2020).
26. L. Poveda-Wong, J. L. Cruz, M. Delgado-Pinar, X. Rosselló-Mechó, A. Díez, and M. V. Andrés, "Fabrication of long period fiber gratings of subnanometric bandwidth," Opt. Lett. **42**(7), 1265–1268 (2017).